



Analysis of Dynamic Fracture Compliance Based on Poroelastic Theory. Part I: Model Formulation and Analytical Expressions

DING WANG,^{1,2} SHOU-LI QU,¹ PING-BO DING,^{3,4} and QUN ZHAO^{1,2}

Abstract—The presence of bedding-parallel fractures at any scale in a rock will considerably add to its compliance and elastic anisotropy. Those properties will be more significantly affected when there is a relatively high degree of connectivity between the fractures and the corresponding interconnected pores. This contribution uses linear poroelasticity to reveal the characteristics of the full frequency-dependent compliance of an infinitely extended fracture model assuming the periodicity of the fractured structures. The fracture compliance tensor is complex-valued due to the wave-induced fluid flow between fractures and pores. The interaction between the adjacent fractures is considered under fluid mass conservation throughout the whole pore space. The quantitative effects of fracture (volume) density (the ratio between fracture thickness and spacing) and host rock porosity are analyzed by the diffusion equation for a relatively low-frequency band. The model in this paper is equivalent to the classical dry linear slip model when the bulk modulus of fluid in the fractures tends to zero. For the liquid-filled case, the model becomes the anisotropic Gassmann's model and sealed saturated linear slip model at the low-frequency and high-frequency limits, respectively. Using the dynamic compliance definition, we can effectively distinguish the saturating fluids in the fractures with the same order magnitude of bulk modulus (e.g., water and oil) using the compliance ratio method. Additionally, the modified dynamic model can be simplified as acceptable empirical formulas if the strain on the fractures induced by the incoming waves is small enough.

Key words: Fracture compliance, porosity, compliance ratio, frequency dependent, poroelastic theory.

1. Introduction

Real rocks are usually permeated by fractures, cracks and joints due to a variety of reasons. Those

geological structures affect the mechanical and hydrological properties of the rock (Nelson 2001). Knowledge of the properties of preferentially oriented fractures in a hydrocarbon reservoir is important for the optimization of production. The tool most frequently used to analyze fracture parameters (size, orientation and density) is the measurement and analysis of seismic wave velocities and energy changes (Maultzsch et al. 2003). A variety of evidences shows that seismic waves are slowed and attenuated because fractures of any scale generally increase rock permeability and elastic compliance (Biot 1956, 1962; Pride et al. 2004; Müller et al. 2010). In non-permeable media, scattering attenuation is the main dissipative mechanism; however, in permeable porous rocks, fluid flow (i.e., fluid–solid friction) is another important form of energy loss. The relation between waves and fluid flow in porous media has been described successfully by poroelastic theory if the rocks are micro-homogeneous at the pore scale (Biot 1956, 1962). However, the wave dispersion and attenuation cannot be described by this classical theory when the rock has specific heterogeneities at pore or larger dimension (e.g., broken pores and fractures).

Analysis of the effective anisotropic elastic tensor of fractured rocks can be divided into two methods: the straightforward effective stiffness approach and the compliance superposition approach. The effective stiffness of fractured media can be obtained by effective medium theory, provided that the wavelength is much longer than the scale of the heterogeneities (pores and fractures). When we take into account the local fluid flow at the scale of the pores or fractures, the elastic parameters show frequency dependence. Le Ravalec and Guéguen (1996)

¹ SINOPEC, Geophysical Research Institute, Nanjing 211103, China. E-mail: wdgeophysics@hotmail.com

² SINOPEC Key Laboratory of Geophysics, Nanjing 211103, China.

³ British Geological Survey, Edinburgh EH9 3LA, UK.

⁴ State Key Laboratory of Petroleum Resource and Prospecting, China University of Petroleum, Beijing 102249, China.

studied the high- and low-frequency elastic moduli for a saturated porous/cracked rock by comparing between self-consistent and poroelastic theories. Hudson (1981) and Hudson et al. (1996) used the so-called ‘method of smoothing’ for the crack problem (Keller 1964). Chapman (2003) derived the effective stiffness of cracked porous media by Eshelby’s ‘interaction energy’ theory (Eshelby 1957). Jakobsen et al. (2003) presented the T-matrix approach to allow for non-dilute concentrations of cracks. In almost all the cases mentioned, the first step in such a calculation requires knowledge of the micro-distribution of inclusions. O’connell and Budiansky presented the elastic moduli of a solid permeated with an isotropic distribution of cracks by use of a self-consistent approximation (O’connell and Budiansky 1974).

The compliance approach is quite popular in recent decades. The effects of aligned fractures on excess effective compliance can be simply reduced to two parameters if the fractures are rotationally invariant about the fracture normal direction: normal compliance and shear compliance, which are associated with pore fluid properties and the structure of the fractures. One important aspect of the compliance is that the ratio of normal compliance to shear compliance helps to identify the petrophysical parameters of fractures and the host matrix (Schoenberg 1980; Liu et al. 2000; Sayers et al. 2009; Verdon and Wüstefeld 2013). Moreover, the compliance formulation can be better understood on a physical perspective and without detailed assumptions concerning the microstructure of the fractures (Schoenberg 1980; Gurevich 2003; Far et al. 2013). At high fracture density, the first-order result written in terms of compliances is closer to the experiment data than the first-order stiffness method (Hudson et al. 2001). However, previous studies were mainly focused on dry fractures and sealed fluid-saturated fractures (fractures embedded in a non-permeable background matrix) (Hudson 1981; Sayers and Kachanov 1995; Schoenberg 1980; Schoenberg and Sayers 1995; Verdon et al. 2008; Sarout and Guéguen 2008). As for the dynamic fracture compliance, the wave-induced fluid flow (WIFF) process among fractures with different fracture mechanics and geometry characteristics has been discussed systematically by Guéguen and Sarout (2009, 2011) and Guéguen and

Kachanov (2011). They mainly assumed that the dynamic fracture compliance and wave dispersion were the result of fracture-to-fracture squirt-flow. When all the fractures have the same geometry and orientation, dispersion is null due to the fact that neighboring fractures would be subjected to the same pore fluid perturbation when a wave propagates through the medium. In contrast, the WIFF effects and frequency dependence can appear when the fractures are randomly oriented. The effects of fluid flow between fractures and pores are analyzed widely using the stiffness approach (Jakobsen et al. 2003; Hudson et al. 1996; Chapman 2003). However, the WIFF process was rarely studied using the compliance approach (Wang 2014). Some efforts thereafter were taken to demonstrate the effects of fluid exchange between different pores in the low/high-frequency limit or in empirical formulas (Gurevich 2003; Adelinet et al. 2011; Brown and Gurevich 2004). Actually, in comparison to sealed fractures, open fractures are more compliant when fluid has time to move between fractures and pores. In other words, fluid flow in porous and fractured media affects significantly the mechanical response of the rock.

Fractures in crustal rocks may exist at a variety of spatial scales, from micro-scale to meter-scale. It has been proven that fractures of all sizes can be the cause of wave anisotropy in rocks (Maultzsch et al. 2003). We are interested in the large-scale fractures, due to the fluid flow in rocks mainly being controlled by this scale of fractures (Maultzsch et al. 2003; Nelson 2001; Liu 2013). The fractures in our study are modeled as infinitely extended and thin poroelastic layers with the different porosity characteristics relative to the host rock (Fig. 1) (Brajanovski et al. 2005, 2006; Lambert et al. 2006; Nakagawa and Schoenberg 2007; Gurevich et al. 2007, 2009; Müller et al. 2010; Wang et al. 2014). In practice, this is a double-porosity dual-permeability model corresponding to a periodically layered poroelastic medium previously studied by White (1975) and Norris (1993). One of the reasons for this postulate for fracture modeling is that the linear slip model (LSM) by Schoenberg (1980) is the basis of our research. We adopt the classical poroelastic theory (Biot 1956) to analyze WIFF and the boundary

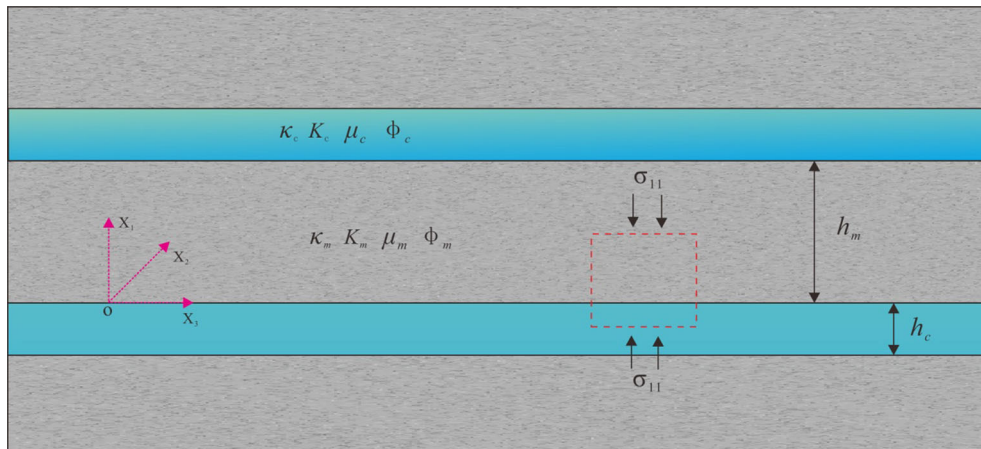


Figure 1
Schematic of perfectly aligned fractures embedded in isotropic porous medium

conditions between the fractures and the pores. This theory is attractive because it allows us to model wave propagation in porous media without specifying individual shapes of grains or pores. We note that the fractures assumed as porous layers is a particular case among all possible fracture populations found in reservoirs. However, this assumption is acceptable if the fractures are mineralized during diagenesis. More importantly, based on previous studies by Brajanovski et al. (2005) and the formulations derived in this paper, there are no restrictions on the assumption (modeling fractures as porous layers) if the fracture thickness is thin enough. Furthermore, the planar porous fracture form has been validated by Lambert et al. (2006) using poroelastic numerical simulations. It is worth noting that in recent years a number of models (whether stiff or compliance approach) related to WIFF are limited mainly to penny-shaped cracks of finite size (Thomsen 1995; Hudson et al. 1996; Tod 2001; Chapman 2003; Guéguen and Sarout 2009, 2011). Comparison between planar fracture model and penny-shaped crack model is discussed in Sect. 4 of this paper and in a companion paper.

In this paper, our goal is to derive the dynamic compliance for poroelastic fractures embedded within a homogeneous isotropic porous background. The effects of wave-induced fluid flow (WIFF) between fractures and pores in fracture deformation are considered. We quantify the pressure distribution in order to obtain the analytic complex-valued compliance of

poroelastic fractures which is a function of fracture density, pore structure and fluid properties.

2. Rock Fracture Model

2.1. Fluid Pressure and Flux Normal to Fracture

A fracture in a porous background matrix can be modeled as an infinite thin porous layer with different petrophysical and hydraulic parameters relative to the matrix (Brajanovski et al. 2005; Gurevich et al. 2009; Wang et al. 2014). So, fractures and the background matrix have a different reaction to an incident wave. A local pressure gradient between fractures and background pores takes place at the interface between different layers. Subsequently, the pore pressure equilibrates with time and this process is governed by pressure diffusion equations in a relatively low-frequency region (Pride 2005; Müller and Rothert 2006; Wang 2014). To illustrate the definition of the fracture problem, we present a simple 1-D heterogeneous model in which fluid flow can be analyzed between two periodic stratified layers with different petrophysical properties as shown in Fig. 1 (x_1 normal to the fracture plane). The subscript index c and m in this paper denote the fractures and the porous background matrix parameters, respectively.

The pressure in the fractured porous medium conforms to the diffusion equation in a fracture periodic

interval $H(h_m + h_c = H)$. We assume that pressure P is a harmonic function of time and can be expressed as $P(x_1, t) = \hat{P}(x_1)e^{-i\omega t}$, where $i = \sqrt{-1}$, ω is the angular frequency, x_1 is the fracture normal direction. The pressure diffusion satisfies the ordinary differential equation $\nabla^2 \hat{P} + \hat{P}i\omega/D = 0$ (Pride 2005; Müller and Rothert 2006), the diffusion parameter $D = \kappa ML/\eta C$, where η is the viscosity coefficient of the pore fluid, $\kappa = \beta \ell^2 \phi^3 / (1 - \phi)^2$ is the permeability based on the Kozeny–Carman equation (Bear 1972; Mavko et al. 1998), $\ell = 22 \times 10^{-5}$ m is the pore or solid particle scale, ϕ is the porosity, $\beta = 0.003$ is a geometrical factor associated with the tortuosity of the pore network (Carcione and Picotti 2006). L is the dry (drained) compressional P-wave modulus, $C = L + \alpha^2 M$ is the compressional P-wave modulus of the fluid-saturated porous medium given by Gassmann's equations (Gassmann 1951; Gurevich 2003). $M = [(\alpha - \phi)/K^s + \phi/K^f]^{-1}$ is the pore space modulus, $\alpha = 1 - K^{\text{dry}}/K^s$ is the Biot–Willis effective stress coefficient (Biot and Willis 1957), K^s and K^f are the bulk modulus of the rock grain and pore fluid, respectively. μ_s is the shear modulus of the rock grain, $K^{\text{dry}} = K^s(1 - \phi)^{3/(1 - \phi)}$ and $\mu^{\text{dry}} = \mu^s(1 - \phi)^{3/(1 - \phi)}$ are the bulk modulus and shear modulus of the skeleton frame (Krief et al. 1990; Brajanovski et al. 2005). However, other relationships between bulk (or shear) modulus and porosity may be chosen, depending on the underlying structure.

The explicit analytical results for the pressure in the fractures and in the background medium were obtained by Wang (2014) and Wang et al. (2014) in the form

$$\hat{P}(\omega, x_1) = \begin{cases} P_c^0 + A_1 e^{\sqrt{\frac{i\omega}{D_c}} x_1} + A_2 e^{-\sqrt{\frac{i\omega}{D_c}} x_1} & -h_c/2 \leq x_1 \leq 0 \\ P_m^0 + B_1 e^{\sqrt{\frac{i\omega}{D_m}} x_1} + B_2 e^{-\sqrt{\frac{i\omega}{D_m}} x_1} & 0 \leq x_1 \leq h_m/2 \end{cases}, \quad (1)$$

where P_c^0 and P_m^0 are the instantaneous initial pressure values in the immediate vicinity of the fracture surface in the fractures and in the background medium, respectively. The origin of the coordinate system is located at the fracture upper surface. The constant coefficients A_1 , A_2 , B_1 , B_2 can be obtained by the boundary conditions at $x_1 = 0$, $-h_c/2$ and $h_m/2$. The relative fluid flow is zero at $x_1 = -h_c/2$ and $x_1 = h_m/2$ due to the symmetry of the problem (the pressure

gradient is zero). At the interface $x_1 = 0$, the fluid pressure and the flux are continuous. We define the fracture and background layer thickness fraction $r_c = h_c/H$ and $r_m = h_m/H$, and all the undetermined coefficients satisfy

$$\begin{cases} A_2 = (P_c^0 - P_m^0)G \\ A_1 = A_2 e^{\sqrt{\frac{i\omega}{D_c}} r_c H} \\ B_1 = A_2 \frac{1 + e^{\sqrt{\frac{i\omega}{D_c}} r_c H}}{1 + e^{\sqrt{\frac{i\omega}{D_m}} r_m H}} + \frac{(P_c^0 - P_m^0)}{1 + e^{\sqrt{\frac{i\omega}{D_m}} r_m H}}, \\ B_2 = B_1 e^{\sqrt{\frac{i\omega}{D_m}} r_m H} \end{cases}, \quad (2)$$

where

$$G = \frac{1}{(1 + e^{\sqrt{\frac{i\omega}{D_m}} r_m H}) \left[\frac{\kappa_c \sqrt{\frac{i\omega}{D_c}} (e^{\sqrt{\frac{i\omega}{D_c}} r_c H} - 1)}{\kappa_m \sqrt{\frac{i\omega}{D_m}} (1 - e^{\sqrt{\frac{i\omega}{D_m}} r_m H})} \right] - (1 + e^{\sqrt{\frac{i\omega}{D_c}} r_c H})}, \quad (3)$$

Equation (3) implies that there is fluid coupling between the fractures and the background matrix. When the permeability of the fracture or that of the host rock tends to zero, then the coupling coefficient $G = 0$, that is, there is no fluid flow in the porous system (Wang 2014).

2.2. Dynamic Compliance of Infinite Parallel Flat Fractures

The quasi-static relationships between wave-induced displacement and stress across a fracture can be obtained if the wavelength is much longer than the local scale lengths of a fracture (such as fracture thickness, spacing, etc.). The displacement discontinuity and the traction vector are linearly related through the excess fracture compliance matrix Z_{ij} based on the infinitesimal strain approximation (Schoenberg 1980; Sayers and Kachanov 1995)

$$[U_i] = Z_{ij} \sigma_j, \quad (4)$$

where $[U] = U^0 - U^{-h_c}$ is the displacement discontinuity vector of the fracture, and σ_j is the effective poroelastic wave stress acting on the fracture. The above relationship is valid in the dry or fluid-saturated condition. If the excess compliance of the fractures is assumed to be invariant with respect to inversion of x_1 , the off-diagonal terms of the compliance matrix are zero, leading to

$$Z = \begin{bmatrix} Z_n & 0 & 0 \\ 0 & Z_t & 0 \\ 0 & 0 & Z_t \end{bmatrix}, \quad (5)$$

where Z_n and Z_t are the normal compliance and shear compliance of a fracture, respectively. They are real valued (frequency independent) and have the dimensions *length/stress* for the sealed and dry fracture cases. In this paper, we assume that the shear strain does not affect fluid flow, so we only verify the effects of fluid exchange on normal compliance (Hudson 1981; Hudson et al. 1996; Gurevich 2003). In order to obtain the fracture normal compliance, we derive the relationship between the fracture normal stress σ_1 and the displacement discontinuity $[U_c^s]_1$ [Eq. (4)]. The volumetric responses based on the Biot theory of porous media are stated as

$$\varepsilon_c = -\frac{1}{K_c^{\text{dry}}} (\sigma - \alpha_c \hat{P}_c), \quad (6)$$

$$\theta_c = -\frac{\alpha_c}{K_c^{\text{dry}}} \left(\sigma - \frac{\hat{P}_c}{\zeta_c} \right), \quad (7)$$

where ε_c and θ_c are the volumetric variations of the solid skeleton and fluid content, respectively. $\sigma = -(\sigma_{11} + \sigma_{22} + \sigma_{33})/3$ is the isotropic compressive stress, ζ_c is the Skempton coefficient of the porous medium (Skempton 1954). Correspondingly, two coupled mechanisms determine the interaction between the fluid and the porous medium: the fluid pressure can compress the rock framework and confining pressure induces a fluid pressure increase in an un-drained configuration. Equations (6) and (7) can be expressed in another form (Wang 2014)

$$\theta_c = \alpha_c \nabla \cdot U_c^s + \frac{\hat{P}_c}{M_c}, \quad (8)$$

where U_c^s is the macroscopic solid average displacement of the fracture. We find that the displacement discontinuity of the fracture is enhanced if the process of fluid flow is considered in Eq. (8). Based on Fig. 1, fluid in the fracture only flows in the x_1 direction because the fracture is isotropic in the x_2 - x_3 plane (global flow and solid skeleton displacement in the fracture plane can be ignored). Then, from Eq. (1) and Darcy's law $S = -\kappa_c \nabla P_c / \eta$, we can obtain the average flux (Wang 2014; Wang et al. 2014)

$$S = -\frac{2\kappa_c}{h_c \eta} A_2 \left(e^{R_c \frac{h_c}{2}} - 1 \right)^2, \quad (9)$$

where $R_c = \sqrt{i\omega/D_c}$ is the inverse of the pressure diffusion length. We assume that the fracture thickness and spacing are much smaller than the wavelength, but much larger than the single grain scale. Thus, we can regard the cube of fracture thickness (the volume of cube is unit base area times fracture thickness height) as the volume element in which the displacement of the solid frame and fluid are averaged. The compressibility of the fluid and the skeleton together affect the pressure diffusion. When the compressibility of the fluid can be ignored, fluid flow is mainly due to the deformation of the solid skeleton. All the above leads to the average flux based on Eq. (1) over the fracture thickness equal to the fluid volumetric variation rate $2S = -\partial\theta_c^1/\partial t$ (θ_c^1 is the relative fluid flow in the normal direction), and therefore the displacement discontinuity of the fracture in the normal direction is given by

$$[U_c^s]_1 = \frac{h_c}{\alpha_c} \left(\frac{\overline{P}_c}{M_c} + \frac{2S}{-i\omega} \right). \quad (10)$$

Pressure within the fracture varies from point to point, and the average pressure in the x_1 direction in Eq. (10) can be expressed as

$$\overline{P}_c = P_c^0 + A_2 \frac{2}{h_c \sqrt{\frac{i\omega}{D_c}}} \left(e^{\sqrt{\frac{i\omega}{D_c}} h_c} - 1 \right), \quad (11)$$

and the pressure in the fracture decreases with time due to the fluid relaxation process ($A_2 < 0$) (Wang 2014). The displacement discontinuity of the fracture is given by

$$[U_c^s]_1 = \frac{h_c}{\alpha_c} \left[\frac{P_c^0}{M_c} + \frac{A_2}{M_c} \frac{2}{h_c \sqrt{\frac{i\omega}{D_c}}} \left(e^{\sqrt{\frac{i\omega}{D_c}} h_c} - 1 \right) + \frac{4\kappa_c}{i\omega \eta h_c} A_2 \left(e^{\sqrt{\frac{i\omega}{D_c}} h_c} - 1 \right)^2 \right], \quad (12)$$

If the wave propagates normal to the fracture, the fracture's instantaneous ($\theta = 0$) initial pressure far from the fracture surface is proportional to the total uniaxial wave stress $P_{c_far}^0 = -\zeta_c^{\text{uni}} \sigma_{11}$ based on the Skempton relationship (Norris 1993; Wang 2000; Brajanovski et al. 2005), where $\zeta_c^{\text{uni}} = \alpha_c M_c / C_c$. Considering the effects of initial pressure (both in

fractures and host rock) far from the fracture surface on fluid flow near the fracture surface, the initial pressure values in the immediate vicinity of the fracture surface in the fractures and background pores are coupled with the P-wave stress (initial pressure in the fractures is uniform due to the small ratio of thickness to wavelength, i.e., $P_{c_far}^0 = P_c^0$) (Johnson 2001)

$$\sigma_{11} = -(P_c^0 - P_m^0)\psi, \quad (13)$$

where

$$\psi = \frac{r_c K_c^{\text{sat}} C_m + r_m K_m^{\text{sat}} C_c}{\alpha_m M_m C_c - \alpha_c M_c C_m} (\zeta_c^{\text{uni}} - \zeta_m^{\text{uni}}). \quad (14)$$

The poroelastic parameter $K^{\text{sat}} = K^{\text{dry}} + \alpha^2 M$ is given by Gassmann's equations (Gassmann 1951). Subsequently, combining the above equations, the dynamic normal compliance is given by the following simplified form

$$[U_c^s]_1 = Z_n \sigma_{11}, \quad (15)$$

where

$$Z_n = \frac{\zeta_c^{\text{uni}} h_c}{M_c \alpha_c} \left\{ 1 + \frac{G}{\psi \zeta_c^{\text{uni}}} \left[\frac{2}{h_c \sqrt{\frac{i\omega}{D_c}}} \left(e^{\sqrt{\frac{i\omega}{D_c}} h_c} - 1 \right) + \frac{4\kappa_c M_c}{i\omega \eta h_c} \left(e^{\sqrt{\frac{i\omega}{D_c}} h_c} - 1 \right)^2 \right] \right\}, \quad (16)$$

Equation (16) is a new expression for the fracture compliance and is the main result of this paper. The compliance is frequency dependent and complex-valued (attenuative). Unless stated otherwise, $\text{Re}[Z_n]$ represents the real part of the normal compliance, while the imaginary part is written as $\text{Im}[Z_n]$. In Eq. (16), $\zeta_c^{\text{uni}} h_c / M_c \alpha_c$ is the high-frequency limit (un-drained condition) of the normal compliance. Because $G < 0$, and $\psi < 0$ for fluid flow from soft fractures to stiff pores, the quantity between the braces is always greater than one and increasing with decreasing frequency, so the dynamic compliance is always larger than the sealed (un-drained) compliance. In the high-frequency limit, $S = 0$ and $\bar{P}_c = P_c^0$, fluid diffusion has not enough time to achieve pressure equilibrium, and the normal compliance is the same as that of the fluid-filled sealed ($\theta_c = 0$) fracture model $Z_n^{\text{high}} = h_c / C_c$, which is consistent

with the definition presented by Nakagawa and Schoenberg (2007). In the low-frequency limit

$$G^{\text{low}} = \frac{-1}{2 \left(\frac{h_c D_m \kappa_c}{h_m D_c \kappa_m} + 1 \right)}, \quad (17)$$

and therefore

$$Z_n^{\text{low}} = \frac{\zeta_c^{\text{uni}} h_c}{M_c \alpha_c} \left[1 - \frac{1}{\psi \zeta_c^{\text{uni}}} \left(\frac{M_c \kappa_c h_c}{2 D_c} + \frac{M_c L_c}{C_c h_c} \right) \right], \quad (18)$$

When we take the limit $h_c \rightarrow 0$, the fracture is hollow ($\phi_c = 1$, $\zeta_c = 1$), so

$$Z_n^{\text{low}} = \frac{\zeta_c^{\text{uni}} h_c}{M_c \alpha_c} \left(1 - \frac{\alpha_m M_m - C_m}{K_m^{\text{sat}}} \frac{1}{\frac{M_m L_m}{C_m h_m} Z_n^{\text{dry}} + 1} \right), \quad (19)$$

and Eq. (19) is similar to Eq. (18) of Brajanovski's paper (Brajanovski et al. 2005), which was based on the conditions of low frequency and thin fracture thickness limits.

The poroelastic parameters of the fractured porous medium used throughout this paper are presented in Table 1.

Figure 2a shows the frequency dependence of the normal compliance of an oil-filled fracture over the full frequency band. The low and high-frequency limits correspond to poroelastic drained and un-drained conditions, respectively. Furthermore, for a fixed (but finite) frequency, when $h_c \rightarrow 0$, the coupling coefficient becomes $^2G = -1/2$ and $\left(e^{\frac{h_c}{\lambda}} - 1 \right) 2A/h_c \gg 4\kappa_c M_c \left(e^{\frac{h_c}{\lambda}} - 1 \right)^2 / i\omega \eta h_c$, so that Eq. (16) can be simplified into

Table 1

List of the constant poroelastic parameters of fractured porous medium used throughout the paper

Variable	Value	SI unit
$K_s \mu_s$	37, 44	GPa
H	1.5	m
$\ell_m \ell_c$	22×10^{-5} , 44×10^{-5}	m
ϕ_c	0.48	—
$\eta_{\text{oil}} \eta_{\text{CO}_2} \eta_{\text{water}}$	5×10^{-3} , 1×10^{-5} , 1×10^{-3}	Pa s
$K_{\text{oil}} K_{\text{CO}_2} K_{\text{water}}$	2.0, 0.0005, 2.25	GPa

The Lamé constants of solid grain are cited from Brajanovski's paper (2005)

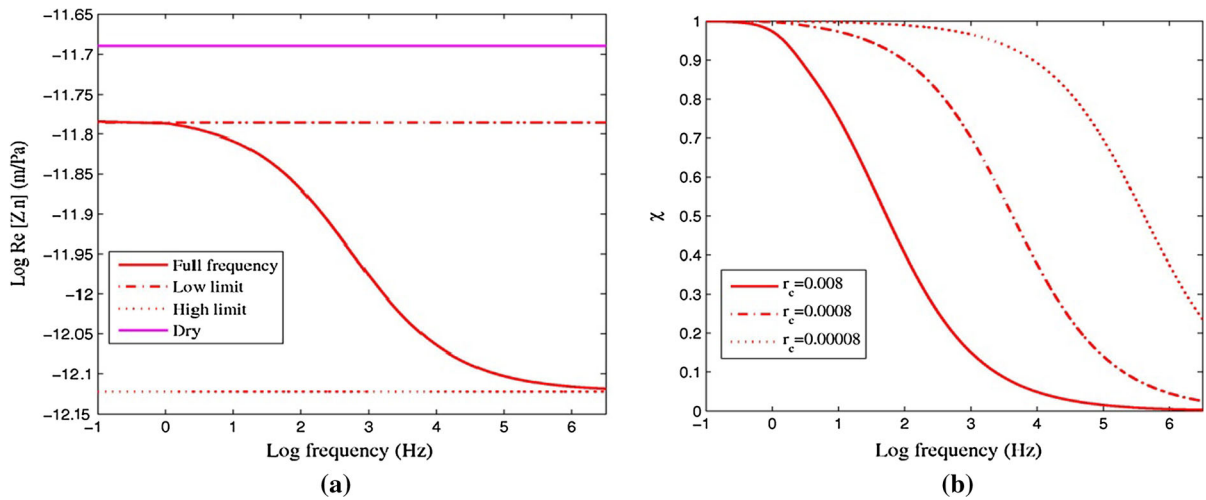


Figure 2

a Oil-filled fracture normal compliance dispersion predicted by full frequency, low-frequency limit, high-frequency limit and dry fracture conditions for $r_c = 0.003$ and $\phi_m = 0.12$. **b** Correction factor χ in Eq. (21) as a function of frequency for various thickness fractions for an oil-filled fracture and $\phi_m = 0.12$

$$Z_n = Z_n^{\text{high}} \left[1 - \frac{A}{\psi h_c} \left(e^{\frac{h_c}{A}} - 1 \right) \right], \quad (20)$$

where $A = \sqrt{D_c/i\omega}$ is the pressure diffusion length in the fractures. Combining Eqs. (16) and (19), we can obtain an analogous empirical expression if the average strain of the fracture is sufficiently small

$$Z_n = Z_n^{\text{high}} + (Z_n^{\text{low}} - Z_n^{\text{high}})\chi, \quad (21)$$

where

$$\chi = \frac{A}{h_c} \frac{G}{G^{\text{low}}} \left(e^{\frac{h_c}{A}} - 1 \right) \quad (22)$$

Figure 2b shows the correction factor from low frequency to high frequency for different (but meeting the $h_c \rightarrow 0$ condition) fracture thicknesses. $\omega \rightarrow 0$ and $\omega \rightarrow \infty$ correspond to $Z_n = Z_n^{\text{low}}$ and $Z_n = Z_n^{\text{high}}$, respectively. Figure 3 shows the difference between the analytical solution [Eq. (16)] and empirical solution [Eq. (21)]. In Fig. 3, the difference of exact (analytical) and approximate (empirical) results increases with the fracture thickness increasing for a fixed frequency. The difference between the two results vanishes with increasing frequency. In this case, the WIFF process does not take place because the wave period is much shorter than the pressure equilibration time. In contrast,

when the frequency is low enough, the difference between the two equations [Eqs. (16), (21)] is obvious because the fractures thickness is small compared to the pressure equilibration length. It is implied that the assumption $h_c \rightarrow 0$ made for the approximate solution is no longer satisfied. In other words, high (low) frequency has the same effects as having thinner (thicker) fractures, which can be perceived by the relationship between fracture thickness and frequency in Eq. (16).

2.3. Characteristic Frequencies of Z_n

Frequency dispersion of the imaginary part of the compliance can be regarded as the frequency dependence characteristics of attenuation (Branjanovski et al. 2005; Gurevich et al. 2009). Based on Eqs. (3) and (16), we derive the asymptotic values of the imaginary part of the compliance, and compare them with pre-existing theoretical results (Branjanovski et al. 2006; Müller and Rotherth 2006).

The behavior of $\text{Im}[Z_n]$ in the generic periodic porous structure exhibits three different frequency regimes separated by two characteristic frequencies (see Appendix 1). For $\omega \rightarrow 0$, the imaginary part of the compliance reduces to

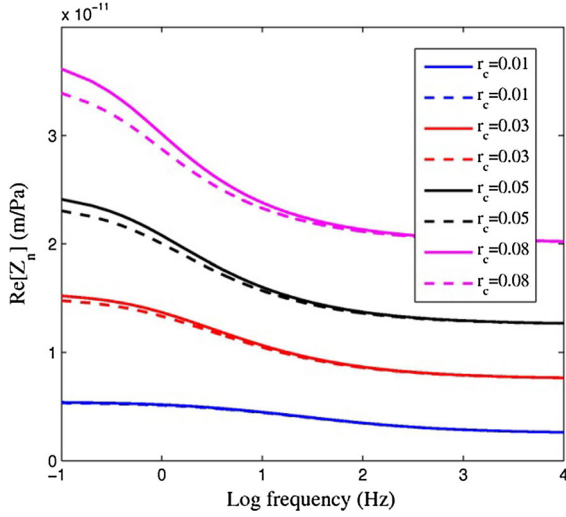


Figure 3

Oil-filled fracture normal compliance dispersion for the analytical and empirical solutions under the different fracture thickness conditions, $r_c = 0.003$, $\phi_m = 0.12$. *Solid and dotted lines* represent exact and approximate solutions, respectively

$$\text{Im}[Z_n] = \omega \frac{h_c}{\psi M_c \alpha_c} \frac{1}{4 D_m \zeta h_m}, \quad (23)$$

This corresponds to the low-frequency asymptote of the compliance, which is proportional to frequency. The intermediate frequency segment of $\text{Im}[Z_n]$ becomes broader for smaller fracture thickness. When $h_c \rightarrow 0$ for a fixed (but finite) frequency, we obtain

$$\text{Im}[Z_n] = \sqrt{\omega} \frac{\alpha_m M_m - C_m}{K_m^{\text{sat}} C_c} h_c^2 \frac{1}{2\sqrt{2D_c}}, \quad (24)$$

Thus, for frequency dispersion of the imaginary part of the compliance is proportional to $\omega^{1/2}$ in the intermediate frequency band. When $\omega \rightarrow \infty$ we obtain

$$\text{Im}[Z_n] = \frac{2}{\sqrt{\omega}} \frac{h_c}{M_c \alpha_c} \frac{1}{\psi} \frac{1}{h_c \sqrt{\frac{1}{D_c} \left(\frac{\kappa_c \sqrt{\frac{1}{D_c}}}{\kappa_m \sqrt{\frac{1}{D_m}}} + 1 \right)}} \quad (25)$$

Consequently, at high frequency the imaginary part of the compliance is proportional to $\omega^{-1/2}$. The behavior can be observed in Figs. 5b, 6b and 7d. Furthermore, the theoretical analysis of the frequency regimes mentioned above is in agreement with published results obtained using different methods (Müller and Rothert 2006; Lambert et al. 2006).

From a physical standpoint, if the thickness of the fracture is small and the frequency is low, the host rock contribution to fluid flow (incoming fluid flow into host rock) is the dominant (see Appendix 2) cause of wave attenuation ($\text{Im}[Z_n]$) because of its relatively long characteristic pressure relaxation time. In this case, the first characteristic frequency of $\text{Im}[Z_n]$ is essentially constant. With the increase of fracture thickness or wave frequency, the flux from the fractures S_c approaches the flux from the host medium S_m , and exceeds S_m finally (see Appendix 2). Since the pressure relaxation time of fractures is always shorter than that of the host medium, the second peak (characteristic frequency) of attenuation ($\text{Im}[Z_n]$) tends to the low-frequency range with the fracture thickness increasing.

3. Results

3.1. Effects of Pore Structure and Physical Properties of Fluids

Based on what has been described above, wave-induced fluid flow in the fracture and its dynamic compliance are influenced by the host rock, the fractures pore structure, and the pore fluid properties simultaneously.

The background porosity is an important parameter controlling the fluid storage capacity of the rock. During the WIFF process, the host rock plays the role of the fluid container (low pressure), while the fracture is the fluid source (high pressure). The matrix porosity ϕ_m can change the normal compliance, as it affects the fluid flow process. Figure 4a–c shows the relationship between the background matrix porosity and the fracture normal compliance $\text{Re}[Z_n]$, the imaginary component of normal compliance $\text{Im}(Z_n)$, and the ratio of normal to shear compliance $\text{Re}[Z_n]/Z_t$ for different fluids. The fracture in the normal direction is similar to an elastic medium when ϕ_m is small enough (no space to store the influx). The curves in Fig. 4a–c show an increase of fracture compliance with the increase of the host rock porosity, and then reach a peak which corresponds to a sufficient pressure equilibrium state (pressure equilibrium time equals the half of the

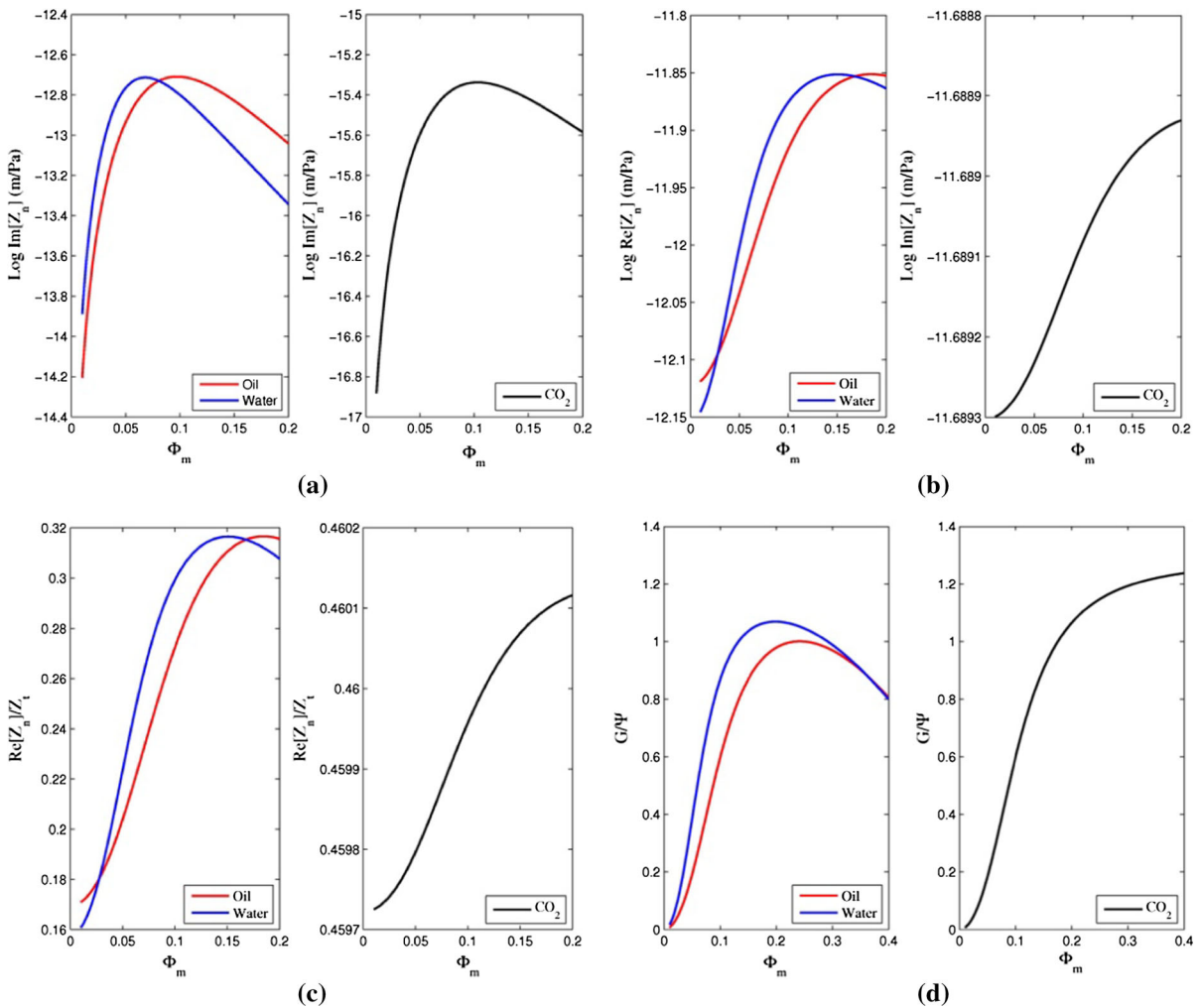


Figure 4

a-d Change of $Re[Z_n]$, $Im(Z_n)$, compliance ratio and G/ψ with respect to ϕ_m for 150 Hz and $r_c = 0.003$ for oil, carbon dioxide and water

wave period) for a fixed frequency. The reason for the curves to decline after this peak is due to the parameter G/ψ in Eq. (16) (Fig. 4d). An analogous tendency can be observed in Fig. 4a–c. From a physics viewpoint, the difference in petrophysical parameters between adjacent layers is decreasing with the increase of ϕ_m (rock is homogeneous when $\phi_m = \phi_c$). The initial pressure in the host rock will be higher than in the fractures if ϕ_m keeps increasing ($\phi_m > \phi_c$) which results in fluid flowing in an opposite direction (flowing from the host rock to the fractures). In this case, the host rock is softer than

the fractures, and the normal compliance is smaller than Z_n^{high} .

Figure 5a shows that the normal compliance $Re[Z_n]$ tends to a finite value in the high-frequency limit regardless of the value of ϕ_m . The fluid is locked in the fractures and has not enough time to equilibrate. However, for the low-frequency limit, the drained compliance is inversely proportional to ϕ_m as the difference of pore properties between fractures and host rock decreases with increasing ϕ_m ($\phi_m < \phi_c$). Therefore, the initial pressure difference decreases and vanishes when $\phi_m = \phi_c$. So the

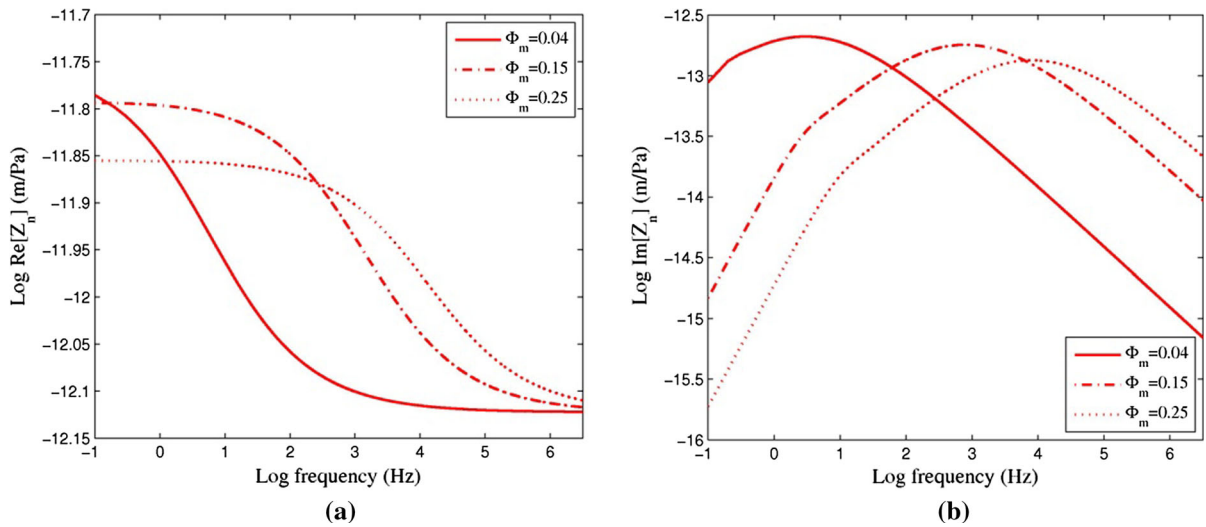


Figure 5

a Oil-filled fracture normal compliance dispersion for various ϕ_m . **b** $\text{Im}[Z_n]$ frequency dependence characteristics under different ϕ_m conditions

wave attenuation associated with the flux of fluid will decrease (see Fig. 5b).

Different pore fluids will yield different results. $M_c = 0$ and $P_c = 0$ when the fluid bulk modulus tends to zero (i.e., dry fracture), so the dry normal compliance is much larger than in the fluid-filled case in the low-frequency limit (anisotropic Gassmann equations). Gas has a weak effect on the fracture compliance, whereas liquids can decrease significantly the excess fracture compliance, especially for sealed (or small diffusion parameter) fractures. Figure 6a shows the dynamic normal compliance dispersion for three fluids with different bulk modulus and viscosity parameters. The bulk modulus of carbon dioxide is much smaller than that of oil and water but cannot be ignored. While fractures filled with gas have a weak dispersion in Fig. 6a when fractures are modeled as poroelastic layers, the dispersion can become more significant if one assumes that the fractures are hollow or the fracture thickness $h_c \rightarrow 0$ (Chapman 2003). Note that a fracture saturated with water has the same normal compliances at the low and high-frequency limits compared with the oil filling case. That is, for the static (un-drained and drained) cases, we cannot distinguish between the normal compliance of water and oil saturated fractures as they have a similar bulk

modulus. Yet this is the drawback of sealed fracture models published previously (Liu et al. 2000; Sayers et al. 2009). The sealed models do not consider the flow between fractures and pores; therefore, the compliance of oil- and water-filled fractures is indistinguishable. In our model, by contrast, the diffusion coefficient D , rather than the bulk modulus can be used to discriminate between oil and water in the fractures in the middle-frequency band.

Wave-induced fluid flow (WIFF) is an important attenuation mechanism in porous media. In our fractured medium model, the imaginary component of the normal compliance $\text{Im}[Z_n]$ may partly reflect wave attenuation characteristics. Thus, Fig. 6b provides information on frequency dependence of seismic wave attenuation. Carbon dioxide has the smallest viscosity and the lowest characteristic frequency, which is in contrast to the conclusions published earlier by Hudson et al. (1996) and Chapman (2003). Previously published models were based on the assumption that fluid flow (pressure diffusion) is controlled by the fluid only (i.e., the fracture is completely hollow). The theoretical basis is the mechanics of viscous fluids rather than poroelasticity. In this paper, we define the pressure diffusion process based on equation $\nabla^2 \hat{P}_c + \hat{P}_c i\omega/D_c = 0$ in the fracture (the fracture is regarded

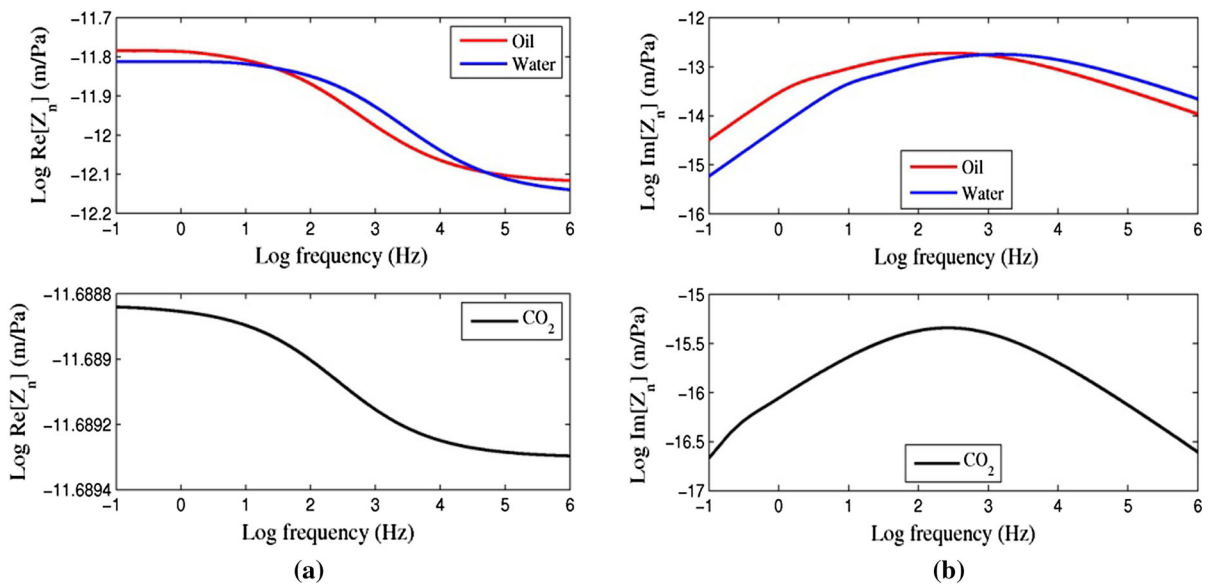


Figure 6

a, b $\text{Re}[Z_n]$ and $\text{Im}[Z_n]$ frequency dependence for oil, carbon dioxide and water, $\phi_m = 0.12$, $r_c = 0.003$

as a porous layer), so D_c is the critical factor that controls pressure diffusion for a fixed fracture thickness (D_m has the same relationship for a different fluid as D_c). Carbon dioxide has the smallest diffusion parameter, so that pressure relaxation is the slowest in this case.

3.2. Effect of Fracture Thickness

The fracture normal compliance associated with viscous flow is a function of the layer thickness and fracture fraction (h_c/H). We define the characteristic time $T^{\text{chara}} = \pi h_c^2 / 4D_c$ for which the pressure diffusion length equals half the fracture thickness. It is proportional to the fracture thickness and is inversely proportional to the diffusion coefficient. The shear compliance is frequency-independent and defined by h_c/μ_c . Figure 7a shows that the normal-to-tangential compliance ratio tends to a fixed value when fracture thickness tends to zero due to the fracture being in a drained condition (wave period is much larger than the diffusion characteristic time). For a fixed r_c , the compliance ratio is inversely proportional to the wave frequency. In contrast, $\text{Re}[Z_n]$ is proportional to the fracture thickness in Fig. 7b). Figure 7c, d shows the $\text{Re}[Z_n]$ and $\text{Im}[Z_n]$ dispersion curves for various

thickness ratios. We find that the $\text{Re}[Z_n]$ dispersion range and the characteristic frequencies of $\text{Im}[Z_n]$ tend to be higher for a thinner fracture. Note that the coordinates of Fig. 7c, d are displayed in log–log scale. The drained and un-drained normal compliance is directly proportional to the thickness (Fig. 7b, c) as mentioned by Brajanovski et al. (2006). As discussed in Sect. 2.3, the behavior of $\text{Im}[Z_n]$ in the generic periodic porosity structure exhibits three different frequency regimes separated by two characteristic frequencies. Moreover, the regime of $\text{Im}[Z_n]$ between the two characteristic frequencies broadens and the peak of $\text{Im}[Z_n]$ decreases with decreasing fracture thickness (Fig. 7d). In Fig. 7d, $\text{Im}[Z_n]$ for different fractions equals each other with increasing frequency (and vanishes in the high-frequency limit). In this case, fluid flowing occurs only in the immediate vicinity of the fracture surfaces.

3.3. Ratio of Normal Compliance to Shear Compliance

Identifying pore fluid types in the fractures and pores of a fractured reservoir is an important goal in the petroleum exploration process. It has already been shown by several authors that the ratio of normal

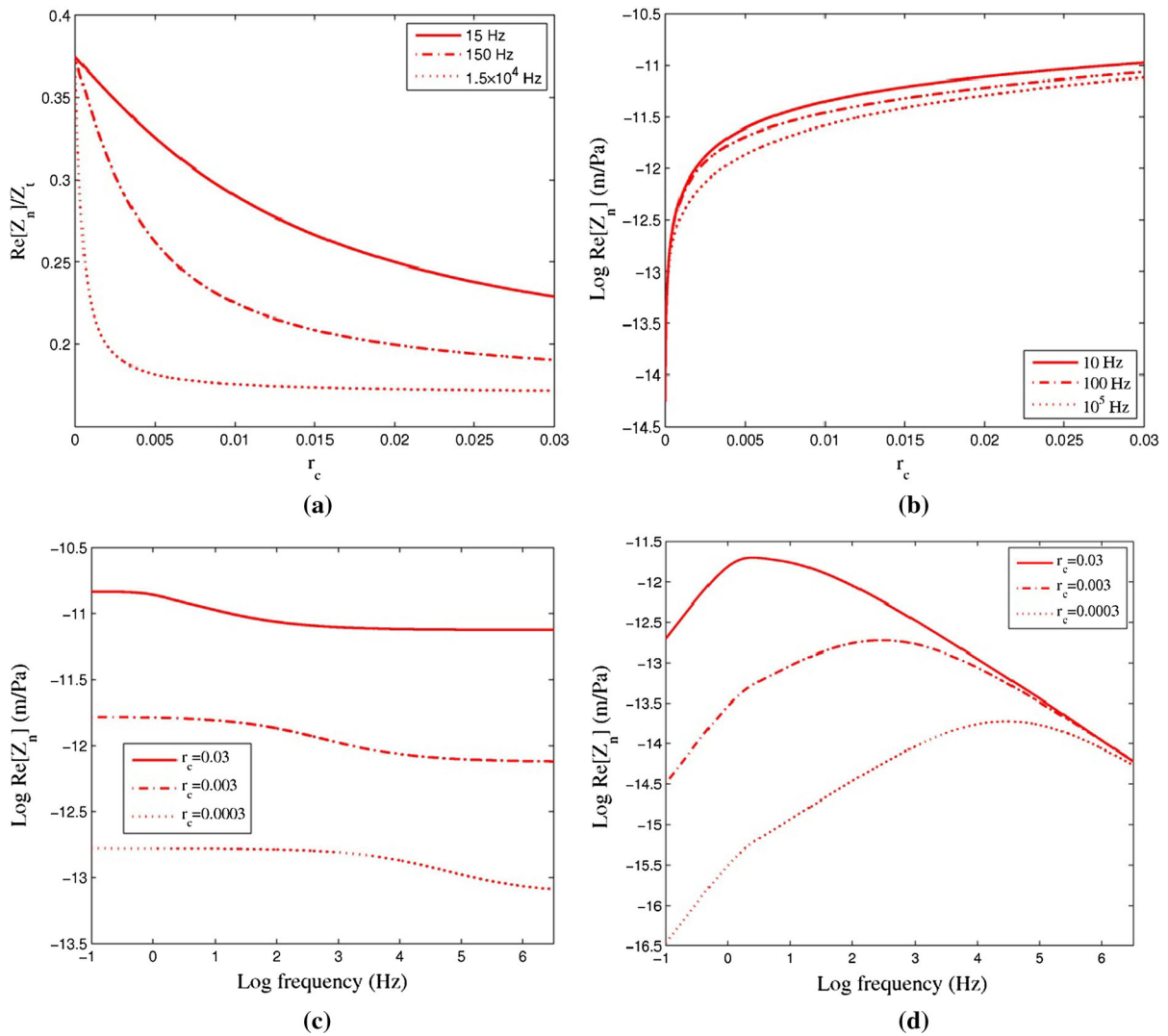


Figure 7

a Oil-filled fracture compliance ratio versus thickness fraction for frequencies 15 Hz, 150 Hz and 15 kHz. **b** Normal compliance versus thickness friction for frequencies 10 Hz, 100 Hz and 0.1 MHz. **c, d** Frequency-dependent $\text{Re}[Z_n]$ and $\text{Im}[Z_n]$, respectively, from the interlayer flow

compliance to shear compliance is an effective and sensitive indicator for discriminating liquid from gas because the introduction of a relatively incompressible fluid into a fracture significantly decreases the normal compliance, but keeps the shear compliance unchanged such that $\text{Re}[Z_n]/Z_t \rightarrow 0$ (Liu et al. 2000; Lubbe et al. 2008; Sayers et al. 2009).

Water and oil are very common in hydrocarbon reservoirs and exist as both single and mixed fluids. From a petrophysical viewpoint, the compliance ratio

method is powerless to distinguish between oil and water in a sealed fracture because they have a similar bulk modulus. However, for an open fracture the fluid viscosity coefficient controls the characteristic time of pressure relaxation. Hence, we can identify different fluids with different viscosity (such as water and oil) based on the compliance ratio.

Figure 8a, b shows a remarkable distinction of compliance ratio between oil and water for the values

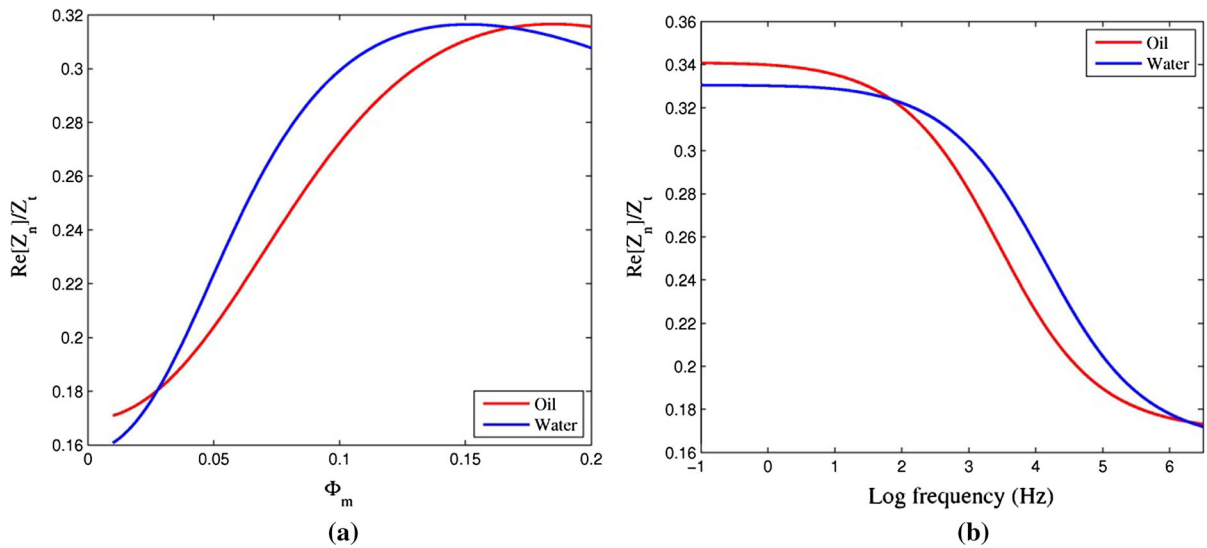


Figure 8

a Change of compliance ratio for oil-filled and water-filled fractures with respect to ϕ_m for 150 Hz and $r_c = 0.003$. **b** Compliance ratio dispersion for oil-filled and water-filled fractures for $\phi_m = 0.2$, and $r_c = 0.003$

of host rock porosity and seismic exploration frequency that we are interested in.

4. Discussion

The use of the concept of dynamic compliance can provide important information on fluid content and lithology of reservoirs. In principle, the WIFF process establishes a relationship between the properties of a porous rock and wave signatures. Fracture compliance increases with porosity up to a peak around to a few per cent porosity (Fig. 4a, b). This peak represents an inherent diffusion equilibrium during wave propagation in the fractured porous medium. Therefore, the magnitude of compliance for a fixed frequency can reflect the background porosity which in turn determines the fluid volume. Note that the wave velocity trend of fractured media versus the host rock porosity can be different from the one shown in Fig. 4a. The reason is that the elastic moduli of the host rock are usually inversely proportional to porosity according to Gassmann equations (Gassmann 1951). Yet in order to obtain wave velocity, the effective elastic moduli of the fractured rock are calculated by inverting the

effective compliance which is a superposition of the compliance of the host rock (inverse of the elastic moduli of the host rock) and the extra compliance of the fractures.

Two characteristic frequencies for a reservoir with periodically spaced fractures described above can be interpreted as a superposition of two coupled fluid flow processes. This may look counter-intuitive, as the previous models for the penny-shaped cracks have a characteristic frequency associated the WIFF process which is a function of crack radius (Dvorkin et al. 1995; Hudson et al. 1996; Chapman 2003). Fluid flow between cracks and pores in published models obeys Darcy's law. Correspondingly, the WIFF process in these models is just calculated from the cracks surfaces to neighboring pores. In this paper, the characteristic lengths for pressure diffusion are the fracture spacing and thickness, rather than the fracture radius. We can predict from Fig. 7d that the second characteristic frequency vanishes when the fracture thickness decreases. Fluid identification is in principle possible with our model. Combining the dynamic compliance and the compliance ratio method, oil can be potentially distinguished from water for a conventional reservoir porosity at seismic frequencies (Fig. 8a, b).

In recent years many of models of attenuation and dispersion due to WIFF have been proposed. Most of these models are limited to finite penny-shaped cracks. We have demonstrated that one can obtain the fracture compliance without abandoning the assumption (i.e., modeling fractures as porous layers) if the fracture thickness is thin enough [Eqs. (16), (19), (20)]. However, the range of fracture porosities for which we can regard fractures as poroelastic layers has not been clearly defined, especially for the fractures of a low degree of mineralization. For completely hollow but finite thickness fractures ($\phi_c = 1$, $h_c = \text{constant}$), we can deal with this problem by two methods that are (1) assuming fractures as planes (no thickness) and considering the WIFF only in the host rock similarly to the popular fracture models with a zero aspect ratio (fractures are infinite) and (2) modeling fractures as a thin layer (without pore structure) saturated with fluids (Liu et al. 2000). For the latter case, the poroelastic theory and viscous fluid mechanics corresponding to the host rock and the fractures, respectively, can be adopted to reveal the pressure diffusion and boundary conditions between the host rock and the fractures (Wang et al. 2016). We need to utilize Navier–Stokes equation to analyze the fluid flow in the hollow fractures (Tang and Cheng 1989; Wang and Zhang 2014).

For simplicity, we usually assume that the fracture (filled with porous material or hollow) has infinite extent and consists of two parallel planes. Therefore, the model that so far have been studied predominantly correspond to the fluid flow between the fractures and the background pores in the fractures normal direction. In practice, real fractures in rocks are inhomogeneous (e.g., the fracture surfaces are rough) along the fracture plane (Sayers et al. 2009), and the WIFF within the fracture is three dimensional (Wang 2014; Wang et al. 2016).

Alternatively, a fracture can be described as a set of discrete penny-shaped cracks (Sayers 1991). The compliances of penny-shaped cracks have been extensively studied in the past few decades (Kachanov 1980; Liu et al. 2000; Sayers et al. 2009). The crack compliance is related to the crack radius and aspect ratio, and to the background matrix properties. The comparison between the porous layer model and penny-shaped crack model is presented by Galvin and

Gurevich (2006) and Gurevich et al. (2009). In the low-frequency limit, the two models are consistent with the fundamental equations of anisotropic Gassmann's theory (Gurevich et al. 2009). Since planar fractures with the same specific surface per unit volume can be expressed through crack density for penny-shaped cracks, the high-frequency attenuation asymptote for the layer model and the penny-shaped crack model are exactly the same (Galvin and Gurevich 2006; Gurevich et al. 2009). In a companion paper, we will systematically discuss that one can establish the quantitative correspondence between the layered fractures and the penny-shaped cracks and illustrate this with the experimental tests.

Finally, it should that be noted the results derived in this paper are only valid for periodically fractured structures. In the normal direction, 1D random media (fracture spacing is a stochastic function) are more realistic in the earth's crust. Further research is required to uncover how to relate the random functions to experimentally significant parameters. The numerical simulation tools for evaluation of effective equivalent rock properties will certainly contribute to this research goal.

5. Conclusions

The behavior of a fractured porous medium is coupled and can be complex. To relate fracture compliance to seismic frequency, a dynamic rock physics model is presented that can describe the effects of the wave-induced fluid flow process on fracture normal compliance. For aligned fractures, the normal compliance in the low and high-frequency limit is equivalent to the results of the anisotropic Gassmann equation and a sealed fluid-filled fracture model, respectively. Furthermore, the examples results show that knowledge of fractures and rock properties of the unfractured host medium are crucial for an accurate description of fracture compliance. We obtain an analogous empirical expression which agrees well with the analytical solution if the fracture thickness is thin enough. The behavior of $\text{Im}[Z_n]$ in a periodically fractured structure exhibits three different frequency regimes separated by two characteristic frequencies.

Based on our model, the compliance ratio method is more efficient for distinguishing fluids with similar bulk modulus but different viscosity. Fractures filled with oil have a significant difference in the compliance ratio dispersion relationship, relative to the water case. For a fixed H and ϕ_c , interlayer flow is controlled by fracture thickness and the background matrix diffusion parameter. Interaction between adjacent fractures is determined by fluid mass conservation. The proposed model is appropriate for high fracture volume density conditions. In future work, the model containing aligned fractures with randomly spacing will continue to be studied.

Acknowledgements

We thank two anonymous reviewers for helping the authors improve the original manuscript. This work is financially supported by the National Basic Research Program of China (973 Program, Grant No. 2014CB239201), the National Science and Technology Major Project of the Ministry of Science and Technology of China (Grant No. 2011ZX05035-001), SINOPEC Research Program (Grant No. P15104).

Appendix 1

Frequency Dependence of Im[Z_n]

The frequency characteristics of Im[Z_n] (attenuation) are associated with the pressure equilibrium process. In this paper, the wave attenuation is controlled two diffusion systems corresponding two characteristic lengths that are fracture spacing and fracture thickness, respectively.

When $\omega \rightarrow 0$, Eq. (3) can be written as

$$G = \frac{-1}{\left(2 + \sqrt{\frac{i\omega}{D_m} h_m}\right) \frac{\kappa_c h_c}{\kappa_m h_m} + \left(2 + \sqrt{\frac{i\omega}{D_c} h_c}\right)}, \quad (26)$$

Using the values in Table 1 for the physical parameters introduced this paper leads to the inequality

$$\xi = \frac{\frac{\kappa_c}{D_c} h_c}{\frac{\kappa_m}{D_m} h_m} \ll 1, \quad (27)$$

We can then derive the imaginary part of the compliance

$$\begin{aligned} \text{Im}[Z_n] &= \text{Im} \left[\frac{h_c}{\psi M_c \alpha_c \left(2 + \sqrt{\frac{i\omega}{D_m} h_m}\right) \xi + \left(2 + \sqrt{\frac{i\omega}{D_c} h_c}\right)} \right] \\ &= \omega \frac{h_c}{\psi M_c \alpha_c 4 D_m \xi h_m} \end{aligned} \quad (28)$$

This means the low-frequency asymptote of the compliance, proportional to frequency. Additionally, the intermediate segment of Im[Z_n] regime becomes broader for smaller fracture thickness. When $h_c \rightarrow 0$ for a fixed (but finite) frequency,

$$\frac{2}{h_c \sqrt{\frac{i\omega}{D_c}}} \left(e^{\sqrt{\frac{i\omega}{D_c} h_c}} - 1 \right) \gg \frac{4\kappa_c M_c}{i\omega \eta h_c} \left(e^{\sqrt{\frac{i\omega}{D_c} h_c}} - 1 \right)^2. \quad (29)$$

Then $G = -1/2$, $\psi = \frac{K_m^{\text{sat}} C_c}{\alpha_m M_m C_c - \alpha_c M_c C_m}$, $\lim_{h_c \rightarrow 0} M_c = \lim_{h_c \rightarrow 0} C_c$ and $a_c = 1$. So Im[Z_n] is given by

$$\text{Im}[Z_n] \approx \text{Im} \left[-\frac{h_c}{M_c \alpha_c} \frac{1}{\psi} \frac{-1}{h_c \sqrt{\frac{i\omega}{D_c}}} \left(h_c \sqrt{\frac{i\omega}{D_c}} + \frac{h_c^2 \frac{i\omega}{D_c}}{2} \right) \right]. \quad (30)$$

Thereby, Eq. (30) reduces to a formula in a frequency-dependent form

$$\text{Im}[Z_n] = \sqrt{\omega} \frac{\alpha_m M_m - C_m}{K_m^{\text{sat}} C_c} h_c^2 \frac{1}{2\sqrt{2D_c}}. \quad (31)$$

That is, the imaginary part of the compliance is proportional to $\omega^{1/2}$ in the intermediate frequency band. Finally, when $\omega \rightarrow \infty$, the following inequality can be obtained

$$\frac{2}{h_c \sqrt{\frac{i\omega}{D_c}}} \left(e^{\sqrt{\frac{i\omega}{D_c} h_c}} - 1 \right) \gg \frac{4\kappa_c M_c}{i\omega \eta h_c} \left(e^{\sqrt{\frac{i\omega}{D_c} h_c}} - 1 \right)^2. \quad (32)$$

Thus, we find immediately that

$$\text{Im}[Z_n] = \text{Im} \left[G \frac{2}{h_c \sqrt{\frac{i\omega}{D_c}}} e^{h_c \sqrt{\frac{i\omega}{D_c}}} \right], \quad (33)$$

meanwhile, when $\omega \rightarrow \infty$

$$G \approx -\frac{1}{\left(\frac{\kappa_c \sqrt{1/D_c}}{\kappa_m \sqrt{1/D_m}} + 1\right) e^{\sqrt{i\omega/D_c} r_c H}}, \quad (34)$$

therefore,

$$\begin{aligned} & \text{Im}[Z_n] \\ &= \text{Im} \left[-\frac{h_c}{M_c \alpha_c \psi} \text{Im} \left[\frac{1}{\left(\frac{\kappa_c \sqrt{1/D_c}}{\kappa_m \sqrt{1/D_m}} + 1\right) e^{\sqrt{i\omega/D_c} r_c H} h_c \sqrt{\frac{i\omega}{D_c}}} \right] \right] \\ &= \frac{2}{\sqrt{\omega}} \frac{h_c}{M_c \alpha_c \psi} \frac{1}{h_c \sqrt{\frac{1}{D_c}} \left(\frac{\kappa_c \sqrt{1/D_c}}{\kappa_m \sqrt{1/D_m}} + 1\right)} \end{aligned} \quad (35)$$

The imaginary part of the compliance is proportional to $\omega^{-1/2}$.

Appendix 2

Fluid Flux Ratio Normal to Fracture

As for the derivation of Eqs. (1–3), fluid flow between the fractures and the background pores can be seen as an inter-coupling process controlled simultaneously by the hydrologic properties of fractures and of the background. Combining Eqs. (1–3) and Darcy's law $V_{\text{flow}} = -\nabla P \frac{\kappa}{\eta}$, we can obtain the fluid flux equation

$$S = -\frac{\kappa_c}{\eta} A_2 \left(e^{\sqrt{\frac{i\omega}{D_c}} h_c/2} - 1 \right)^2 + \frac{\kappa_m}{\eta} B_1 \left(e^{\sqrt{\frac{i\omega}{D_m}} h_m/2} - 1 \right)^2, \quad (36)$$

Then the flux ratio between fracture and matrix $\zeta = \frac{S_c}{S_m}$ is

$$\zeta = -\frac{\kappa_c A_2 \left(e^{R_c h_c/2} - 1 \right)^2}{\kappa_m B_1 \left(e^{R_m h_m/2} - 1 \right)^2}, \quad (37)$$

In the low-frequency limit, the flux ratio is $h_c/h_m \ll 1$ according to Eq (36). The pore pressure gradient is a constant in the whole pore structure. The flux ratio is $\sqrt{D_c/D_m} \gg 1$ in the high-frequency limit, indicating that the WIFF only occurs near the fractures planes. Therefore, we can conclude that the total flux mainly comes from host rock in the low-frequency limit while from fracture in the high-frequency limit.

REFERENCES

- Adelinet, M., Fortin, J., & Guéguen, Y. (2011). Dispersion of elastic moduli in a porous-cracked rock: Theoretical predictions for squirt-flow. *Tectonophysics*, 503(1), 173–181.
- Bear, J. (1972). *Dynamics of fluid in porous media*. New York: Elsevier.
- Biot, M. A. (1956). Theory of elastic waves in a fluid-saturated porous solid. I. Low frequency range. *Journal of the Acoustic Society of America*, 28, 168–178.
- Biot, M. A. (1962). Mechanics of deformation and acoustic propagation in porous media. *Journal of Applied Physics*, 33, 1482–1498.
- Biot, M. A., & Willis, D. G. (1957). The elastic coefficients of the theory of consolidation. *Journal of Applied Mechanics*, 24, 594–601.
- Brajanovski, M., Gurevich, B., & Schoenberg, M. (2005). A model for P-wave attenuation and dispersion in a porous medium permeated by aligned fractures. *Geophysical Journal International*, 163(1), 372–384.
- Brajanovski, M., Müller, T. M., & Gurevich, B. (2006). Characteristic frequencies of seismic attenuation due to wave-induced fluid flow in fractured porous media. *Geophysical Journal International*, 166(2), 574–578.
- Brown, L., & Gurevich, B. (2004). Frequency-dependent seismic anisotropy of porous rocks with penny-shaped cracks. *Exploration Geophysics*, 35(2), 111–115.
- Carcione, J. M., & Picotti, S. (2006). P-wave seismic attenuation by slow-wave diffusion: Effects of inhomogeneous rock properties. *Geophysics*, 71(3), O1–O8.
- Chapman, M. (2003). Frequency-dependent anisotropy due to meso-scale fractures in the presence of equant porosity. *Geophysical Prospecting*, 51(5), 369–379.
- Dvorkin, J., Mavko, D., & Nur, A. (1995). Squirt flow in fully saturated rocks. *Geophysics*, 60, 97–107.
- Eshelby, J. D. (1957). The determination of the elastic field of an ellipsoidal inclusion and related problems. In *Proceedings of the Royal Society of London a mathematical, physical and engineering sciences* (Vol. 241, pp. 376–396). London: The Royal Society.
- Far, M. E., Sayers, C. M., Thomsen, L., Han, D. H., & Castagna, J. P. (2013). Seismic characterization of naturally fractured reservoirs using amplitude versus offset and azimuth analysis. *Geophysical Prospecting*, 61(2), 427–447.
- Galvin, R. J., & Gurevich, B. (2006). Interaction of an elastic wave with a circular crack in a fluid-saturated porous medium. *Applied Physics Letters*, 88, 061918.
- Gassmann, F. (1951). Über die Elastizität poröser Medien. *Vierteljahrsschrder der Naturforschenden Gessellschaft in Zürich*, 96, 1–23.
- Guéguen, Y., & Kachanov, M. (2011). Effective elastic properties of cracked and porous rocks. In *Mechanics of crustal rocks*, CISM Courses and Lectures (Vol. 533). Berlin: Springer.
- Guéguen, Y., & Sarout, J. (2009). Crack-induced anisotropy in crustal rocks: predicted dry and fluid-saturated Thomsen's parameters. *Physics of the Earth and Planetary Interiors*, 172(1), 116–124.
- Guéguen, Y., & Sarout, J. (2011). Characteristics of anisotropy and dispersion in cracked medium. *Tectonophysics*, 503(1), 165–172.

- Gurevich, B. (2003). Elastic properties of saturated porous rocks with aligned fractures. *Journal of Applied Geophysics*, 54(3), 203–218.
- Gurevich, B., Brajanovski, M., Galvin, R. J., Müller, T. M., & Toms-Stewart, J. (2009). P-wave dispersion and attenuation in fractured and porous reservoirs—poroelasticity approach. *Geophysical Prospecting*, 57(2), 225–237.
- Gurevich, B., Galvin, R. J., Brajanovski, M., Müller, T. M., & Lambert, G. (2007). Fluid substitution, dispersion and attenuation in fractured and porous reservoirs—Insights from new rock physics models. *Leading Edge*, 26(9), 1162–1168.
- Hudson, J. A. (1981). Wave speeds and attenuation of elastic waves in material containing cracks. *Geophysical Journal of the Royal Astronomical Society*, 64, 133–150.
- Hudson, J. A., Liu, E., & Crampin, S. (1996). The mechanical properties of materials with interconnected cracks and pores. *Geophysical Journal International*, 124(1), 105–112.
- Hudson, J. A., Pointer, T., & Liu, E. (2001). Effective-medium theories for fluid-saturated materials with aligned cracks. *Geophysical Prospecting*, 49(5), 509–522.
- Jakobsen, M., Hudson, J. A., & Johansen, T. A. (2003). T-matrix approach to shale acoustics. *Geophysical Journal International*, 154(2), 533–558.
- Johnson, D. L. (2001). Theory of frequency dependent acoustics in patchy-saturated porous media. *Journal of the Acoustic Society of America*, 110(2), 682–694.
- Kachanov, M. (1980). Continuum model of medium with cracks. *Journal of the Engineering Mechanics Division*, 106, 1039–1051.
- Keller, J. B. (1964). Stochastic equations and wave propagation in random media. *Proceedings of Symposia in Applied Mathematics*, 16, 145–170.
- Krief, M., Garat, J., Stellingwerff, J., & Ventre, J. (1990). A petrophysical interpretation using the velocities of P and S waves (full-wave sonic). *The Log Analyst*, 5, 355–369.
- Lambert, G., Gurevich, B., & Brajanovski, M. (2006). Attenuation and dispersion of p-waves in porous rocks with planar fractures: Comparison of theory and numerical simulations. *Geophysics*, 71, N41–N45.
- Le Ravalec, M., & Guéguen, Y. (1996). High- and low-frequency elastic moduli for a saturated porous/cracked rock-differential self-consistent and poroelastic theories. *Geophysics*, 61(4), 1080–1094.
- Liu, E. (2013). *Seismic fracture characterization: Concepts and practical applications*. Cambridge: Academic Press.
- Liu, E., Hudson, J. A., & Pointer, T. (2000). Equivalent medium representation of fractured rock. *Journal Geophysical Research*, 105(B2), 2981–3000.
- Lubbe, R., Sothcott, J., Worthington, M. H., & McCann, C. (2008). Laboratory estimates of normal and shear fracture compliance. *Geophysical Prospecting*, 56(2), 239–247.
- Maultzsch, S., Chapman, M., Liu, E., & Li, X. Y. (2003). Modelling frequency-dependent seismic anisotropy in fluid-saturated rock with aligned fractures: implication of fracture size estimation from anisotropic measurements. *Geophysical Prospecting*, 51(5), 381–392.
- Mavko, G., Mukerji, T., & Dvorkin, J. (1998). *The Rock physics handbook: Tools for seismic analysis of porous media*. Cambridge: Cambridge University Press.
- Müller, T. M., Gurevich, B., & Lebedev, M. (2010). Seismic wave attenuation and dispersion resulting from wave-induced flow in porous rocks—A review. *Geophysics*, 75(5), 75A147–75A164.
- Müller, T. M., & Rothert, E. (2006). Seismic attenuation due to wave-induced flow: Why Q in random structures scales differently. *Geophysical Research Letters*, 33(16), L16305.
- Nakagawa, S., & Schoenberg, M. A. (2007). Poroelastic modeling of seismic boundary conditions across a fracture. *Journal of the Acoustic Society of America*, 122(2), 831–847.
- Nelson, R. A. (2001). *Geologic analysis of naturally fractured reservoirs* (2nd ed.). London: Butterworth-Heinemann.
- Norris, A. N. (1993). Low-frequency dispersion and attenuation in partially saturated rocks. *Journal of the Acoustic Society of America*, 94(1), 359–370.
- O'Connell, R. J., & Budiansky, B. (1974). Seismic velocities in dry and saturated cracked solids. *Journal Geophysical Research*, 79(35), 5412–5426.
- Pride, S. R. (2005). Relationships between seismic and hydrological properties. In *Hydrogeophysics* (pp. 253–290). Netherlands: Springer.
- Pride, S. R., Berryman, J. G., & Harris, J. M. (2004). Seismic attenuation due to wave-induced flow. *Journal of Geophysical Research Solid Earth*, 109(B1).
- Sarout, J., & Guéguen, Y. (2008). Anisotropy of elastic wave velocities in deformed shales: Part 2-modeling results. *Geophysics*, 73, D91–D103.
- Sayers, C. M. (1991). Fluid flow in a porous medium containing partially closed fractures. *Transport in Porous Media*, 6(3), 331–336.
- Sayers, C. M., & Kachanov, M. (1995). Microcrack-induced elastic wave anisotropy of brittle rocks. *Journal Geophysical Research*, 100(B3), 4149–4156.
- Sayers, C. M., Taleghani, A. D., & Adachi, J. (2009). The effect of mineralization on the ratio of normal to tangential compliance of fractures. *Geophysical Prospecting*, 57(3), 439–446.
- Schoenberg, M., & Sayers, C.M. (1995). Seismic anisotropy of fractured rock. *Geophysics*, 60(1), 204–211.
- Schoenberg, M. (1980). Elastic wave behavior across linear slip interfaces. *Journal of the Acoustic Society of America*, 68(5), 1516–1521.
- Skempton, A. W. (1954). The pore-pressure coefficients A and B. *Geotechnique*, 4(4), 143–147.
- Tang, X. M., & Cheng, C. H. (1989). A dynamic model for fluid flow in open borehole fractures. *Journal Geophysical Research*, 94(B6), 7567–7576.
- Thomsen, L. (1995). Elastic anisotropy due to aligned cracks in porous rock. *Geophysical Prospecting*, 43, 805–829.
- Tod, S. R. (2001). The effects on seismic waves of interconnected nearly aligned cracks. *Geophysical Journal International*, 146, 249–263.
- Verdon, J. P., Angus, D. A., Michael, K. J., & Hall, S. A. (2008). The effect of microstructure and nonlinear stress on anisotropic seismic velocities. *Geophysics*, 73(4), D41–D51.
- Verdon, J. P., & Wüstefeld, A. (2013). Measurement of the normal/tangential fracture compliance ratio (Z_n/Z_t) during hydraulic fracture stimulation using S-wave splitting data. *Geophysical Prospecting*, 61(s1), 461–475.
- Wang, H. F. (2000). *Theory of linear poroelasticity with application to geomechanics and hydrogeology*. Princeton: Princeton University Press.
- Wang, D. (2014). *Theory of elastic waves in heterogeneous fractured porous media* [in Chinese with English abstract]. Ph. D. Thesis, University of Chinese Academy of Sciences.

- Wang, D., Wang, L. J., & Ding, P. B. (2016). The effects of fracture permeability on acoustic wave propagation in the porous media: A microscopic perspective. *Ultrasonics*, *70*, 266–274.
- Wang, D., Wang, L. J., & Zhang, M. G. (2014). Analysis of the attenuation characteristics of an elastic wave due to the wave-induced fluid flow in fractured porous media. *Chinese Physics Letters*, *31*(4), 044301.
- Wang, D., & Zhang, M. G. (2014). Elastic wave propagation characteristics under anisotropic squirt-flow condition. *Acta Physica Sinica*, *63*(6), 69101. **(in Chinese with English abstract)**.
- White, J. E. (1975). Computed seismic speeds and attenuation in rocks with partial gas saturation. *Geophysics*, *40*, 224–232.

(Received April 8, 2015, revised February 27, 2017, accepted March 1, 2017, Published online March 10, 2017)